Anomalous foreshock activity in southern California is associated with zones of high heat flow

Ester Manganiello[1,1], Marcus Herrmann[2,2], and Warner Marzocchi[3,3]

[1]University of study Naples Federico II
[2]University of Naples 'Federico II'
[3]The University of Naples Federico II

November 30, 2022

Abstract

Foreshock analysis promises new insights into the earthquake nucleation process and could potentially improve earthquake forecasting. Well-performing clustering models like the Epidemic-Type Aftershock Sequence (ETAS) model assume that foreshocks and general seismicity are generated by the same physical process, implying that foreshocks can be identified only in retrospect. However, several studies have recently found higher foreshock activity than predicted by ETAS. Here, we revisit the foreshock activity in southern California using different statistical methods and find anomalous foreshock sequences, i.e., those unexplained by ETAS, mostly for mainshock magnitudes below 5.5. The spatial distribution of these anomalies reveals a preferential occurrence in zones of high heat flow, which are known to host swarm-like seismicity. Outside these regions, the foreshocks generally behave as expected by ETAS. These findings show that anomalous foreshock sequences in southern California do not indicate a pre-slip nucleation process, but swarm-like behavior driven by heat flow.

1   **New physical implications from revisiting foreshock activity in southern California**

2   **Ester Manganiello[1], Marcus Herrmann[1], and Warner Marzocchi[1]**

3   [1]Dipartimento di Scienze della Terra, dell'Ambiente e delle Risorse, Università degli
4   Studi di Napoli 'Federico II', Naples, Italy
5
6   Corresponding author: E. Manganiello, ester.manganiello@unina.it
7

8   **Key Points:**

9   • We compare the foreshock activity in southern California with the prediction of the best-
10   performing earthquake clustering model.
11   • Sequences with an anomalous excess of foreshocks are associated mostly with moderate
12   mainshocks and preferentially with high heat flow.
13   • The prevalence of anomalous foreshock sequences in zones of high heat flow does not
14   support the pre-slip nucleation model.

Abstract

Foreshock analysis promises new insights into the earthquake nucleation process and could potentially improve earthquake forecasting. Well-performing clustering models like the Epidemic-Type Aftershock Sequence (ETAS) model assume that foreshocks and general seismicity are generated by the same physical process, implying that foreshocks can be identified only in retrospect. However, several studies have recently found higher foreshock activity than predicted by ETAS. Here, we revisit the foreshock activity in southern California using different statistical methods and find anomalous foreshock sequences, i.e., those unexplained by ETAS, mostly for mainshock magnitudes below 5.5. The spatial distribution of these anomalies reveals a preferential occurrence in zones of high heat flow, which are known to host swarm-like seismicity. Outside these regions, the foreshocks generally behave as expected by ETAS. These findings show that anomalous foreshock sequences in southern California do not indicate a pre-slip nucleation process, but swarm-like behavior driven by heat flow.

Plain Language Summary

Many studies have observed that large earthquakes are preceded by smaller events, called foreshocks. If they have distinctive characteristics that make them recognizable in an ongoing sequence in real time, they can significantly improve the forecasting capability of large earthquakes. To investigate the nature of foreshocks, we compare real seismicity with the expectation of the most skilled earthquake clustering model, which assumes that foreshocks do not have any distinctive characteristics with respect to general seismicity. We find that discrepancies between reality and expectation mostly affect foreshock sequences that anticipate moderate mainshocks with magnitudes below 5.5. We show that those anomalous foreshock sequences tend to occur where the heat flow is high, which are already known for the occurrence of swarm-like sequences. Outside these regions, the observed foreshock activity is explained well by the clustering model. These findings indicate that anomalous foreshock sequences are not diagnostic of impending large earthquakes but are influenced by the heat flow.

1 Introduction

It is well known that many large earthquakes are preceded by smaller events (e.g., 1999 M7.6 Izmit, Turkey (Bouchon et al., 2011; Ellsworth & Bulut, 2018), 2009 M6.1 L'Aquila, Italy (Chiaraluce et al., 2011), 2011 M9.0 Tohoku, Japan (Kato et al., 2012), 2019 M7.1 Ridgecrest, USA (Meng & Fan, 2021)), which are (a posteriori) called foreshocks. The role of foreshocks in earthquake predictability can be epitomized by two still debated conceptual hypotheses about earthquake nucleation: the "pre-slip model" versus the "cascade model" (Ellsworth & Beroza, 1995; Gomberg, 2018). According to the former, foreshocks are diagnostic precursors, because they are triggered by an aseismic slip that precedes large earthquakes; in the latter model, foreshocks are like any other earthquake, which trigger one another, with one of them eventually becoming exceedingly larger (the mainshock).

Notwithstanding the still active debate on these hypotheses, seismologists are not yet able to recognize foreshocks in real-time, tacitly implying that foreshocks are not different from the rest of seismicity, indirectly supporting the cascade model. This view is further supported by the fact that the current best performing short-term earthquake forecasting model (Taroni et al., 2018)—the Epidemic-Type Aftershock Sequences (ETAS; Ogata, 1988) model—assumes that foreshocks, mainshocks, and aftershocks are undistinguishable and governed by the same

58 process. ETAS belongs to the class of branching point process models known in the statistical
59 literature as Hawkes or self-exciting point processes: every earthquake can trigger other
60 earthquakes according to established empirical relations, with their magnitudes being
61 independent from past seismicity. In essence, ETAS implicitly acknowledges the cascade model
62 and its good forecasting performance makes ETAS an appropriate null hypothesis.

63 Instead, if foreshocks are dominated by mechanisms other than earthquake triggering, as the pre-
64 slip model expects, they could be distinguished from general seismicity and potentially increase
65 the probability for a larger earthquake to follow. Several studies recently investigated foreshock
66 sequences of southern California and found that they deviate from expectations of the classical
67 ETAS model with spatially invariant parameters. For example, Seif et al. (2019), Petrillo and
68 Lippiello (2021), and Moutote et al. (2021) find, albeit at varying degrees, a higher foreshock
69 activity in real seismicity than in synthetic catalogs simulated with ETAS. Hence, ETAS appears
70 to be unable to predict all the observed seismicity, which may suggest that foreshocks are distinct
71 from general seismicity and governed by different mechanisms. These findings provide hope that
72 foreshocks are distinguishable and could pave the way to significantly improved earthquake
73 predictability.

74 Here we reexamine foreshock activity in southern California and investigate the existence and
75 main characteristics of foreshock sequences that cannot be explained by ETAS, i.e., anomalous
76 foreshock sequences. In other words, we look for evidence against the cascade model. To make
77 the results comparable to previous analyses, we use an ETAS model with spatially invariant
78 triggering parameters. We perform two different statistical tests and consider the potential
79 influence of subjective choices, such as the method to identify mainshocks and their foreshocks.
80 To fathom the main characteristics of possible anomalous foreshock sequences, we investigate
81 different magnitude classes and analyze the spatial correlation with heat flow as a physical
82 parameter. With our findings, we aim to contribute to improving earthquake forecasting and the
83 understanding of earthquake nucleation processes.

84 2 Data and Methods

85 We use the relocated earthquake catalog for southern California catalog (Hauksson et al., 2012,
86 see Data Availability Statement), selecting all earthquakes with $M \geq 2.5$ from 1-1-1981 to 31-
87 12-2019 except nuclear events (i.e., at the Nevada Test site) from the catalog, totaling 47'574
88 events.

89 Because there is no absolute and precise procedure to identify mainshocks, foreshocks, and
90 aftershocks, the way of analyzing a catalog and distinguishing these events is unavoidably
91 subjective (Molchan & Dmitrieva, 1992; Zaliapin et al., 2008). To mitigate this subjective
92 choice, we analyze the catalog using two quite different techniques: the Nearest-Neighbor (NN)
93 clustering analysis proposed by Baiesi and Paczuski (2004) and elaborated by Zaliapin et al.
94 (2008), and the spatiotemporal windows (STW) method (Agnew and Jones, 1991; Marzocchi
95 and Zhuang, 2011; Seif et al., 2019).

96 The NN method operates in a space-time-magnitude domain based on the NN distance η_j, i.e.,
97 the space-time-magnitude distance between event j and all earlier events i that is minimal. The
98 event i with the shortest distance to event j is called NN, or parent, event. By assigning a parent
99 event to each event j, all events become associated with another. To identify individual families
100 (i.e., sequences) or single events, we use the same threshold $\eta_0 = 10^{-5}$ as Zaliapin et al.

101 (2008), which effectively removes event associations with too large η_j. For each sequence, we
102 refer to the event with the largest magnitude as the mainshock and all associated events that
103 occur before it as its foreshocks. We only consider sequences with foreshocks and ignore those
104 that have no foreshocks.
105

106 For the STW method, we initially consider all events with magnitude $M \geq 4$ as possible
107 mainshocks. Then, we exclude events that are (i) preceded by a larger event within a
108 spatiotemporal window of 10 km and 3 days; (ii) preceded by an event with $M > 5$ within 100
109 km and 180 days; and (iii) not preceded by at least one event within 10 km and 3 days. For the
110 remaining mainshocks, all preceding events within a window of 10 km and 3 days are considered
111 foreshocks.

112 To simulate synthetic catalogs, we use the ETAS model of K. Felzer (Felzer et al., 2002, see
113 Data Availability Statement and supporting information Text S1 and Table S1) with spatially
114 invariant triggering parameters given by Hardebeck et al. (2008, see Table S2). Using an
115 available ETAS model reduces potential influences from subjective parameter choices. We
116 verify its overall reliability by comparing the number of events in the real catalog with the
117 distribution of simulated events in the synthetic catalogs (see Text S2 and Figures S1 and S2),
118 finding that the ETAS model is consistent with the observation.

119 Once the mainshocks and their foreshocks have been identified in both the real and 1000
120 synthetic catalogs, we compare their foreshock statistics using two approaches named TEST1
121 and TEST2. The two tests are described in detail below; both use the cascade model, which is
122 implied by ETAS, as null hypothesis but emphasize different aspects of the problem. TEST1
123 involves the average number of observed foreshocks per sequence, whereas TEST2, which has
124 been inspired by the work of Seif et al. (2019), involves the frequency of observing a certain
125 number of foreshocks per sequence. We apply both tests to various mainshock magnitude classes
126 $C_M = \{4.0 \leq m_M < 4.5, 4.5 \leq m_M < 5.0, 5.0 \leq m_M < 5.5, 5.5 \leq m_M < 6.0, m_M \geq 6.0\}$ and
127 foreshock magnitude thresholds $T_F = \{m_F \geq 2.5, m_F \geq 3.0, m_F \geq 3.5, m_F \geq 4.0\}$; these choices
128 are based on Seif et al. (2019), but we add the class $4.0 \leq m_M < 4.5$ to C_M. Although we report
129 statistical test results, we do not formally account for applying the tests multiple times; the
130 results are therefore meant to indicate possible patterns of (apparently) anomalous foreshock
131 activity.

132 In TEST1, the null hypothesis under test $H_0^{(1)}$ is that the average number of foreshocks in the real
133 catalog is not larger than the corresponding quantity in the synthetic catalogs. For each
134 mainshock magnitude class $c \in C_F$ and each foreshock magnitude threshold $t \in T_F$, we count the
135 number of mainshocks (with foreshocks), N_M^{real}, and the number of foreshocks N_F^{real} in the real
136 catalog; N_F^{real} is normalized by N_M^{real} to obtain $\widehat{N}_F^{real}$. We calculate the same quantity for each
137 synthetic catalog and build its empirical cumulative distribution function (eCDF); if $\widehat{N}_F^{real}$ is
138 above the 99th percentile of the eCDF, we reject $H_0^{(1)}$ at a significance level of 0.01.

139 In TEST2, the null hypothesis under test $H_0^{(2)}$ is that for each number of foreshocks, $N_F > 0$, the
140 frequency of observed cases is not larger than the frequency in synthetic catalogs. For each $c \in$
141 C_M and each $t \in T_F$, we count the number of mainshocks that have a certain N_F and normalize it
142 by N_M^{real}. In this way, we obtain the probability mass function (PMF) for the real catalog as a
143 function of N_F. Then, we apply the same procedure to each synthetic catalog and obtain 1000

144   synthetic PMFs, for which we calculate the 99th percentile at each N_F. Finally, at each N_F, we
145   reject $H_0^{(2)}$ at a significance level of 0.01 if the corresponding PMF value of the real catalog is
146   larger than the 99th percentile (i.e., when the real catalog contains more foreshock sequences with
147   this specific N_F than expected by ETAS). In essence, TEST2 seeks anomalies at every N_F,
148   whereas TEST1 could be seen as a cumulative version of TEST2.

149   Based on the results of the tests, we can label each foreshock sequence as 'anomalous' or
150   'normal' using an intuitive approach: for TEST1, if the null hypothesis is rejected for a certain
151   class, all foreshock sequences with a N_F larger than the 99th percentile of the eCDF in that class
152   are labeled as 'anomalous' (and 'normal' otherwise); for TEST2, if the null hypothesis is
153   rejected for a specific N_F, all sequences with this N_F are labeled as 'anomalous' (and 'normal'
154   otherwise). Effectively, a foreshock sequence in $c \in C_M$ is labeled 'anomalous' if it is
155   'anomalous' in at least one class $t \in T_F$. For TEST1, we argue that the approach is conservative,
156   because comparing a single sequence against the average behavior of foreshock sequences may
157   lead to wrongly label more actual normal foreshock sequences as 'anomalous' (i.e., false
158   positives) than wrongly labeling anomalous foreshock sequences as 'normal' (i.e., false
159   negatives). To investigate this aspect, we perform an alternative analysis by building two eCDFs
160   of N_F (i.e., without normalizing by N_M): one for the real catalog (eCDF[real]) and one for all
161   synthetic catalogs combined (eCDF[ETAS]). If the 99th percentile of eCDF[real] is larger than the
162   corresponding percentile of eCDF[ETAS] in a certain class, we label each foreshock sequence as
163   'anomalous' whose N_F is above the 99th percentile of eCDF[ETAS].

164   To investigate the physical interpretation of possible anomalous foreshock sequences in the real
165   catalog, we analyze their spatial distribution. Specifically, taking inspiration from Zaliapin and
166   Ben-Zion (2013), we create a map by interpolating heat flow measurements (see Data
167   Availability Statement) with a radial smoothing approach ($r = 20$ km) to acknowledge areas
168   without data. For each foreshock sequence, we extract the interpolated heat flow value closest to
169   the mainshock location if it is within r, otherwise we discard the sequence. Then we test if the
170   distribution of extracted heat flow values is significantly different for normal and anomalous
171   foreshock sequences. If pre-slip is responsible for anomalous foreshock sequences, we should
172   not find any difference, i.e., a spatial pattern. We employ two statistical tests: the two-sample
173   Kolmogorov-Smirnov test (null hypothesis: the two distributions have the same parent
174   distribution), and the paired Wilcoxon test (null hypothesis: the two distributions have the same
175   median). In essence, the Kolmogorov-Smirnov test is sensitive to any kind of difference between
176   both distributions, whereas the Wilcoxon test is sensitive to one distribution having higher values
177   than the other.

178   3 Results

179   3.1 Testing for anomalous foreshock activity

180   Figure 1 shows the results of TEST1 using NN to identify mainshocks and their foreshocks; the
181   results using STW are reported in supporting information Figure S3. Each subplot shows a
182   comparison of the eCDF based on synthetic catalogs with the observed value from the real
183   catalog for each class in C_M and T_F. As shown in Figure 1 and Figure S3, TEST1 rejects $H_0^{(1)}$,
184   i.e., identifies anomalous foreshock sequences, exclusively for mainshock magnitudes $m_M <$
185   5.5. Of a total of 152 foreshock sequences, we find 61 (40%) to be anomalous; with the STW
186   method we find 143 foreshock sequences of which 34 (23%) are anomalous (all with $m_M <$

187 5.5.). Using instead the alternative analysis without normalizing by N_M (Figure S4), we find 19
188 (12.5%) to be anomalous, which suggests that TEST1 overestimated the number of anomalies
189 due to using averages, as anticipated in Data and Methods.

190 Figure 2 shows the results of TEST2 for each class in C_M and T_F using the NN method; the
191 results using the STW method are reported in supporting information Figure S5. Most PMF
192 values of the real catalog are not anomalous because they are below the 99th percentile of
193 synthetic PMF values. We find 21 of 152 (14%) foreshock sequences to be anomalous, most of
194 which are again associated with $m_M < 5.5$ (only three have larger m_M). Using the STW method
195 we find 10 of 143 (7%) foreshock sequences to be anomalous.

196 For comparison, Figure 2 also reports the results obtained by applying the approach of Seif et al.
197 (2019), which tests a similar yet different null hypothesis than TEST2. Specifically, they treat all
198 synthetic catalogs as one single compound catalog. In this way, the PMF is normalized with a
199 much larger number of mainshocks than a single catalog (e.g., like the real catalog); for an
200 increasing number of synthetic catalogs, the PMF decreases progressively observation (i.e.,
201 lowering the detectable minimum frequency) and moves further away from the real. In other
202 words, our TEST2 honors the fact that a finite earthquake catalog must have a lower detectable
203 frequency of foreshocks in the PMF; this lower frequency depends on the number of mainshocks
204 that have foreshocks, which in turn depends on the length of the earthquake catalog (the lowest
205 frequency is 1 out of the number of mainshocks that have foreshocks). In addition, the approach
206 of Seif et al. (2019) normalizes the PMF by the total number of mainshocks that have foreshocks
207 (N_M, as we do in TEST2) *and* no foreshocks, which further reduces the PMF by another 0.5–1
208 order of magnitude depending on $c \in C_M$.

209 We repeated TEST1 and TEST2 at a 0.05 significance level (i.e., 95th percentile), which was
210 originally used by Seif et al. (2019), see supporting information (Text S3 and Figures S6 and
211 S7).

212 3.2 Correlating foreshock sequences with the heat flow

213 To investigate the physical cause of anomalous foreshock sequences we inspect the correlation
214 of their locations with the local heat flow. We choose this property because previous papers
215 suggested that the heat flow relates to statistical properties of seismic sequences (e.g., Enescu et
216 al., 2009, Chen & Shearer, 2016; Ross et al., 2021; Zaliapin & Ben-Zion, 2013).

217 Figures 3a and 4a overlay the locations of normal and anomalous foreshock sequences identified
218 by TEST1 and TEST2, respectively, on a heat flow map. Figures 3b and 4b show the
219 corresponding eCDFs of the interpolated heat flow observed at the locations of normal and
220 anomalous foreshock sequences. In both cases, anomalous foreshock sequences tend to occur
221 more frequently at locations of higher heat flow than normal sequences. This trend is confirmed
222 by the *p*-values of the two-sample Kolmogorov-Smirnov and paired Wilcoxon tests (see
223 annotations in Figures 3b and 4b), which are below 0.05, indicating that the two samples come
224 from different parent distributions with different means. Figures 3 and 4 are based on the NN
225 method to identify mainshocks and their foreshocks; the results based on the STW method
226 confirm our findings (see supporting information Figures S8 and S9), as do the results based on a
227 0.05 significance level (Figures S10 and S11). Moreover, TEST1-based results are stable even if
228 we use the alternative procedure to identify anomalous foreshock sequences using eCDFs
229 without normalizing by N_M (see Figure S12).

230   We verify the stability of our results using foreshock anomalies identified by Petrillo and
231   Lippiello (2021). The authors provided us locations of their identified normal and anomalous
232   foreshock sequences (G. Petrillo, pers. comm., 2022), letting us apply our analysis on a dataset
233   that is completely independent from our assumptions and modeling choices. The results shown in
234   Figure S13 confirm our findings of a preferential occurrence of foreshock anomalies in zones of
235   high heat flow.

236   Finally, we add a word of caution on the interpretation of the results, that is, the spatial coverage
237   of heat flow data compared to the earthquake activity is rather incomplete in northern Mexico.
238   For instance, several anomalous foreshock sequences occur in this area but cannot be included in
239   the heat flow analysis due to the lack of heat flow measurements. In addition, the available heat
240   flow measurements in northern Mexico are not consistent with the Geothermal map of North
241   America (Blackwell & Richards, 2004), which indicates a generally high heat flow (> 100
242    $\mu W/m^2$) in this area along the San Andreas Fault.

4 Discussion & Conclusion

244   We have found that foreshocks have the same characteristics of general seismicity as expected
245   by ETAS, except for some cases. Our finding is in general agreement with previous studies of
246   foreshock activity, all of which found (with some important differences not discussed here)
247   higher foreshock activity than expected (Chen & Shearer, 2016; Moutote et al., 2021; Petrillo &
248   Lippiello, 2021; Seif et al., 2019). However, our results additionally show that foreshock
249   anomalies are mostly associated with mainshock magnitudes below 5.5—independently from the
250   two tests and the two procedures to identify mainshocks and their foreshocks. Moreover, these
251   anomalies are located preferentially (and statistically significant) in zones of high heat flow. The
252   combination of these two findings suggests that sequences with anomalous foreshock activity
253   behave more like seismic swarms. In fact, independent studies (e.g., Enescu et al., 2009, Chen &
254   Shearer, 2016; Ross et al., 2021; Zaliapin & Ben-Zion, 2013) have shown that swarm-like
255   activity is common in those areas where we have found anomalous foreshock sequences.

256   Our results do not allow us to further elucidate why foreshock anomalies correlate with high heat
257   flow. The anomalies may be driven by specific physical mechanisms (e.g., actual seismic
258   swarms mostly driven by fluids) or still relate to a cascade model that is not spatially uniform.
259   The latter may be better described by an ETAS model with spatially varying triggering
260   parameters. In fact, Enescu et al. (2009) and Nandan et al. (2017) show that some parameters of
261   a spatially varying ETAS model (which mostly depend on the more abundant aftershocks)
262   correlate with the heat flow in southern California. Such a more elaborated clustering model
263   implies more active foreshock sequences where the heat flow is high, which agrees with our
264   empirical findings based on the analysis of (less abundant) foreshocks.

265   Conversely, foreshock sequences located in zones of lower heat flow predominantly behave as
266   expected, i.e., in agreement with the null hypothesis given by the ETAS model. Since it is
267   reasonable to assume that a pre-slip model should not be severely affected by heat flow, our
268   results do not indicate the pre-slip model as a major candidate to explain the anomalous
269   foreshock behavior in southern California. It goes without saying that our results do not prove
270   the cascade model as the truth, but that they do not bring any evidence against it and in favor of
271   the pre-slip model.

272 Our results also highlight the importance of analyzing seismic sequences in zones of high heat
273 flow in more detail, especially to understand the physical reasons of anomalous foreshock
274 sequences: Are they related to seismic swarms with an implicit limitation to the mainshock
275 magnitude? Or are they related to different clustering processes than those driving tectonic
276 sequences? The difference is crucial, in particular regarding the forecasting of large earthquakes.

277 Our findings raise an urgent need to find (quasi-)real-time methods to discriminate swarm-like
278 from ETAS-like sequences. Such a discrimination method could lead to significant
279 improvements in earthquake forecasting, because being able to identify a swarm-like sequence as
280 such could markedly reduce the forecast probability for a large earthquake. We note that an
281 interesting attempt in this direction has been made by Zaliapin and Ben-Zion (2013), who found
282 that swarm-like sequences have a different topologic tree structure (i.e., an internal clustering
283 hierarchy, which connects background and triggered earthquakes). Unfortunately, this method
284 can currently only be used retrospectively, limiting its applicability in earthquake forecasting.
285 We envision other possible parameterizations of the topologic tree structure that may facilitate its
286 use from a forecasting perspective.

Acknowledgments

Open Research

294 The southern California catalog of Hauksson et al. (2012) was obtained from
295 https://scedc.caltech.edu/data/alt-2011-dd-hauksson-yang-shearer.html, version "1981–2019"
296 (last accessed April 2021). Heat flow data were obtained from the following sources: National
297 Geothermal Data System (http://geothermal.smu.edu/static/DownloadFilesButtonPage.htm, last
298 accessed May 2021) using the data sets '*Aggregated Well Data*', '*Heat Flow Observation in
299 Content Model Format*', '*SMU Heat Flow Database of Equilibrium Log Data and Geothermal
300 Wells*', and '*SMU Heat Flow Database from BHT Data*'; and RE Data Explorer (https://www.re-
301 explorer.org/re-data-explorer/download/rede-data, last accessed May 2021) for northern Mexico.
302 The ETAS simulator of K. Felzer was obtained from
303 https://web.archive.org/web/20200712004939/https://pasadena.wr.usgs.gov/office/kfelzer/AftSi
304 mulator.html, last accessed February 2022). The alternative dataset of normal and anomalous
305 foreshock locations was provided by G. Petrillo (pers. comm., 2022). The methods to perform
306 our foreshocks analyses are available as MATLAB code at DOI: 10.5281/zenodo.6376221
307 and https://gitlab.com/ester.manganiello/foreshock-analyses.
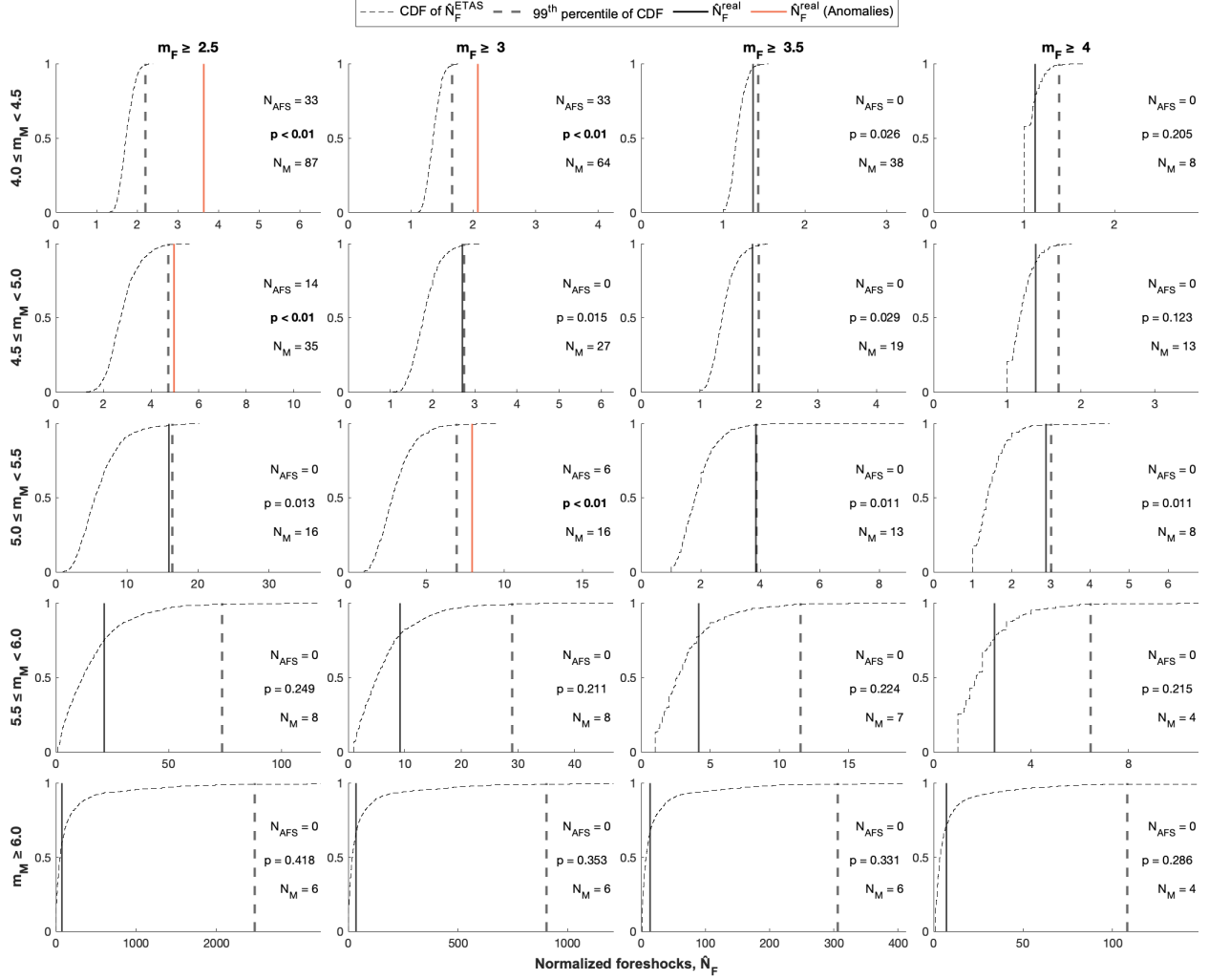
Figure 1. Results of TEST1 for various classes of the mainshock magnitude m_M (rows) and thresholds for the foreshock magnitude m_F (columns). Each subplot displays the number of normalized foreshocks $\widehat{N}_F$ for the real catalog (vertical lines; red if anomalous, black otherwise) and the empirical Cumulative Distribution Functions (eCDFs, dashed curves) with its 99th percentile (dashed vertical lines) for 1000 synthetic catalogs. Each subplot also reports the number of anomalous foreshock sequences, N_{AFS}, the p-value for TEST1, and the number of mainshocks, N_M. The results are based on the NN method; supporting information Figure S3 shows results based on the STW method. Note that each subplot uses a different N_F-axis range to account for the varying data range.
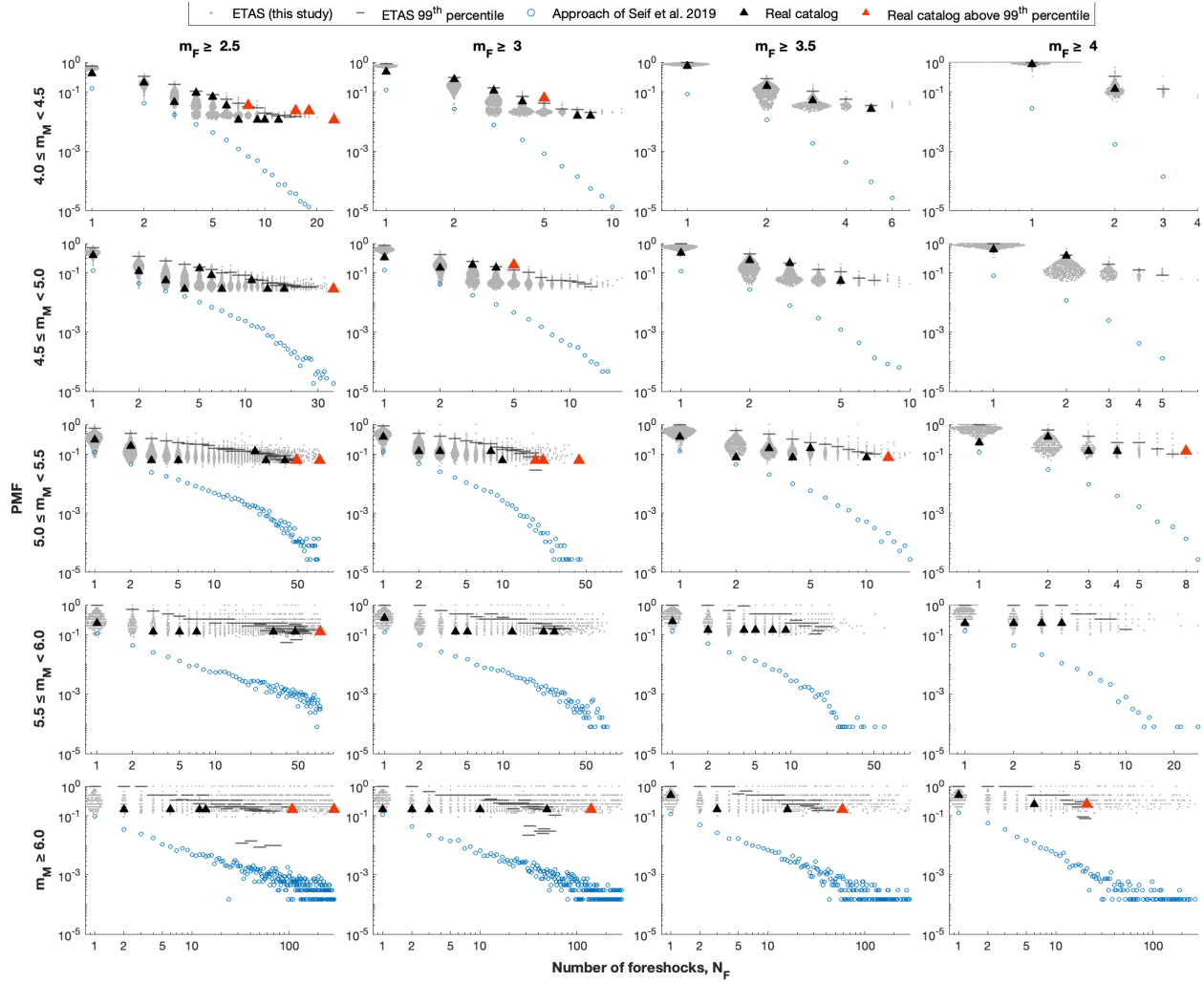
Figure 2. Results of TEST2 showing probability mass functions (PMFs) of the number of foreshocks N_F for various classes of m_M (rows) and m_F (columns). The PMFs are shown for (i) the real catalog (triangles), (ii) all synthetic catalogs (small gray dots as swarm distributions) with their 99th percentile (gray horizontal bars), and (iii) when considering all synthetic catalogs as a single compound catalog (blue open circles, using the approach of Seif et al., 2019). Triangles become red when they are located above the 99th percentile of (ii). The results are based on the NN method to identify mainshocks and their foreshocks; supporting information Figure S5 shows results based on the STW method. Note that each subplot uses a different N_F-axis range.
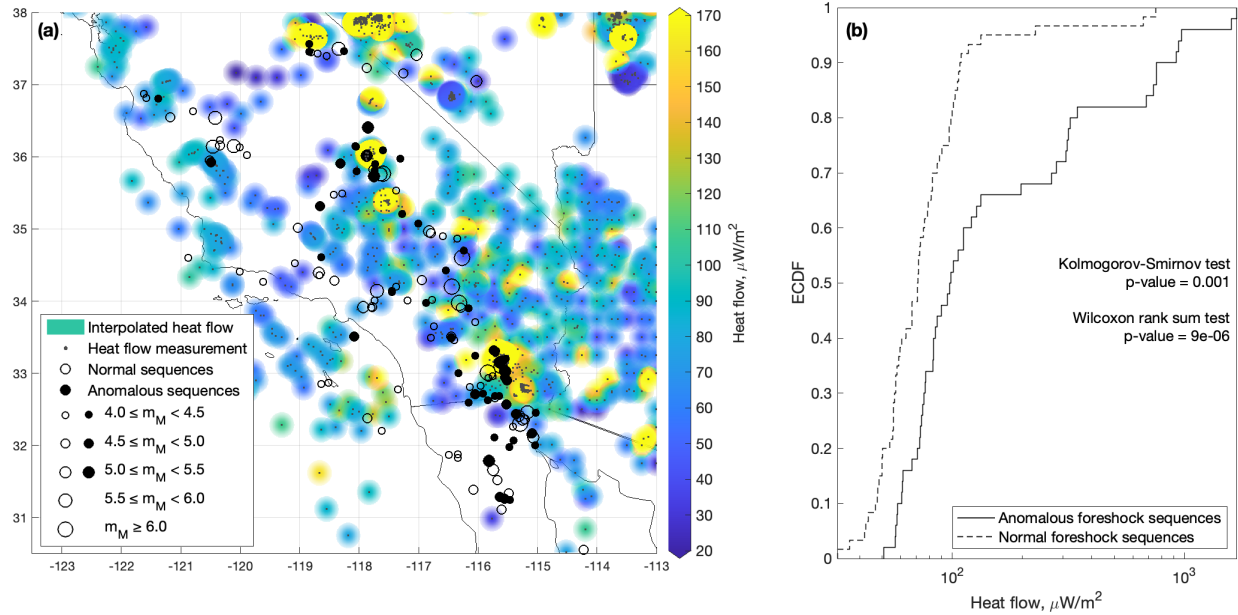
Figure 3. Correlating foreshock sequences with the heat flow. (a) Locations of normal (empty circles) and anomalous foreshock sequences (filled circles) identified with TEST1 overlayed on a heat flow map. The circles sizes scales with m_M (see legend). The interpolated heat flow map is based on sampled heat flow measurements (small gray dots, see Data and Methods section); (b) eCDFs of heat flow values at locations of normal (dashed curve) and anomalous foreshock sequences (solid curve); both eCDFs are compared using two statistical tests (see annotation with corresponding *p*-values). The results are based on the NN method; supporting information Figure S8 shows results based on the STW method.
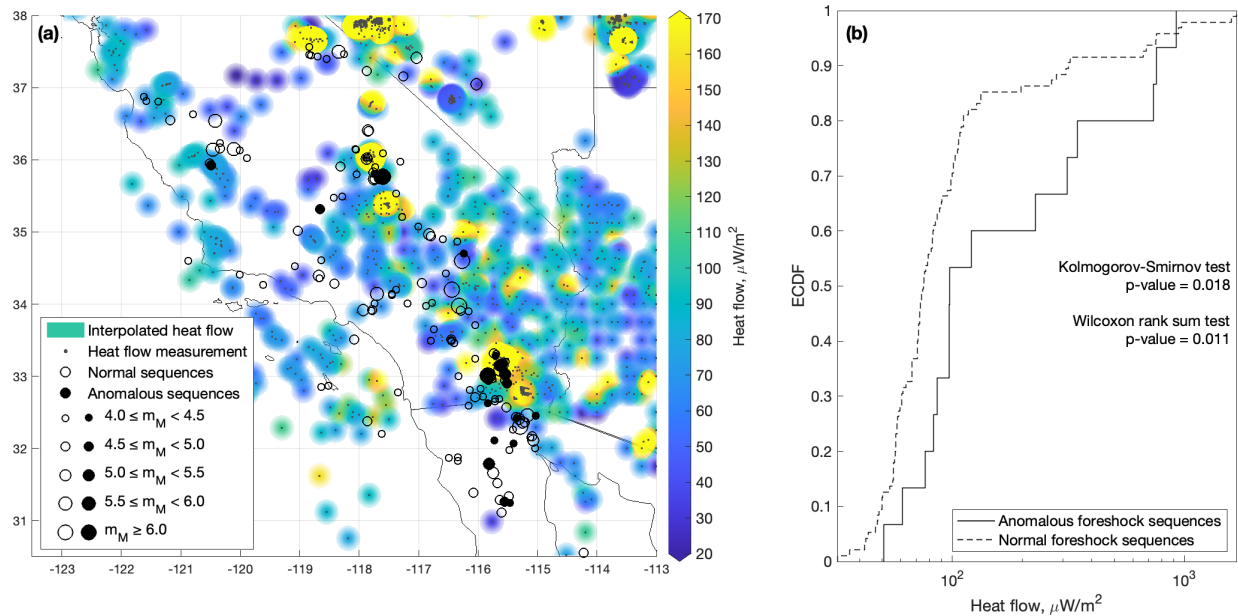
Figure 4. Like Figure 3 but with foreshock sequences labeled as 'anomalous' or 'normal' using TEST2. Supporting information Figure S9 shows results based on the STW method.

341 **References**

342 Agnew, D. C., & Jones, L. M. (1991). Prediction probabilities from foreshocks. *Journal of*
343   *Geophysical Research, 96*(B7), 11959. https://doi.org/10.1029/91JB00191
344 Baiesi, M., & Paczuski M. (2004). Scale-free networks of earthquakes and aftershocks. *Physical*
345   *Review E*, *69*, 066106. https://doi.org/10.1103/PhysRevE.69.066106.
346 Blackwell, D. D., & Richards, M. (2004). Geothermal Map of North America, AAPG Map, scale
347   1:6,500,000, Product Code 423. url: https://www.smu.edu/-
348   /media/Site/Dedman/Academics/Programs/Geothermal-
349   Lab/Graphics/Geothermal_MapNA_7x10in.gif
350 Bouchon, M., Karabulut, H., Aktar, M., Özalaybey, S., Schmittbuhl, J., & Bouin, M. P. (2011).
351   Extended Nucleation of the 1999 Mw 7.6 Izmit Earthquake. *Science*, *331*(6019), 877–
352   880. https://doi.org/10.1126/science.1197341
353 Chen, X. & Shearer, P. M. (2016). Analysis of Foreshock Sequences in California and
354   Implications for Earthquake Triggering. *Pure Applied Geophysical*, *173*(1), 133–152.
355   https://doi.org/10.1007/s00024-015-1103-0
356 Chiaraluce, L., Chiarabba, C., De Gori, P., Di Stefano, R., Improta, L., Piccinini, D.,
357   Schlagenhauf, A., Traversa, P., Valoroso, L., & Voisin, C. (2011). The 2009 L'Aquila
358   (central Italy) seismic sequence. *Bollettino di Geofisica Teorica ed Applicata*, *52*(3), 367-
359   387. https://doi.org/10.4430/bgta0019
360 Ellsworth, W. L., & Beroza, G. C. (1995). Seismic Evidence for an Earthquake Nucleation
361   Phase. *Science*, *268*, 851-855. https://doi.org/10.1126/science.268.5212.851
362 Ellsworth, W. L., & Bulut, F. (2018). Nucleation of the 1999 Izmit earthquake by a triggered
363   cascade of foreshocks. *Nature Geoscience*, *11*(7), 531–535.
364   https://doi.org/10.1038/s41561-018-0145-1
365 Enescu, B., Hainzl, S., and Ben-Zion, Y. (2009). Correlations of Seismicity Patterns in Southern
366   California with Surface Heat Flow Data. *Bulletin of the Seismological Society of*
367   *America*, *99* (6), 3114-3123. https://doi.org/10.1785/0120080038
368 Felzer, K. R., Becker, T. W., Abercrombie, R. E., Ekström, G., & Rice, J. R. (2002). Triggering
369   of the 1999 M_w 7.1 Hector Mine earthquake by aftershocks of the 1992 M_w 7.3 Landers
370   earthquake. *Journal of Geophysical Research*, *107*(B9), 2190.
371   https://doi.org/10.1029/2001JB000911
372 Gomberg, J. (2018). Unsettled earthquake nucleation. *Nature Geoscience*, 11(7), 463–464.
373   https://doi.org/10.1038/s41561-018-0149-x
374 Hardebeck, J. L., Felzer, K. R., & Michael, A. J. (2008). Improved tests reveal that the
375   accelerating moment release hypothesis is statistically insignificant. *Journal of*
376   *Geophysical Research*, *113*, 3B08310. https://doi.org/10.1029/2007JB005410
377 Hauksson, E., Yang, W., & Shearer, P. M. (2012). Waveform relocated earthquake catalog for
378   Southern California (1981 to June 2019). *Bulletin of the Seismological Society of*
379   *America*, *102*(5), 2239–2244. https://doi.org/10.1785/0120120010
380 Kato, A., Obara, K., Igarashi, T., Tsuruoka, H., Nakagawa, S., & Hirata, N. (2012). Propagation
381   of Slow Slip Leading Up to the 2011 Mw 9.0 Tohoku-Oki Earthquake. *Science*,
382   *335*(6069), 705-708. https://doi.org/10.1126/science.1215141
383 Marzocchi, W., & Zhuang, J. (2011). Statistics between mainshocks and foreshocks in Italy and
384   Southern California. *Geophysical Research Letters*, *38*(9), 2011GL047165.
385   https://doi.org/10.1029/2011GL047165

386   Meng, H., & Fan, W. (2021). Immediate foreshocks indicating cascading rupture developments
387   for 527 M 0.9 to 5.4 Ridgecrest earthquakes. *Geophysical Research Letters*, *48*,
388   e2021GL095704. https://doi.org/10.1029/2021GL095704

389   Molchan, G. M., & Dmitrieva, O. E. (1992). Aftershock identification: methods and new
390   approaches. *Geophysical Journal International*, *109*(3), 501–516.
391   https://doi.org/10.1111/j.1365-246X.1992.tb00113.x

392   Moutote, L., Marsan, D., Lengliné, O., & Duputel, Z. (2021). Rare occurrences of non-cascading
393   foreshock activity in Southern California. *Geophysical Research Letters*, *48*,
394   e2020GL091757. https://doi.org/10.1029/2020GL091757

395   Nandan, S., Ouillon, G., Wiemer, S., and Sornette, D. (2017). Objective estimation of spatially
396   variable parameters of epidemic type aftershock sequence model: Application to
397   California, *Geophysical Research Letters Solid Earth*, *122*, 5118–5143.
398   https://doi.org/10.1002/2016JB013266

399   Ogata, Y. (1988). Statistical models for earthquake occurrences and residual analysis for point
400   processes. Journal of the American Statistical Association, 83 (401), 9-27.
401   https://doi.org/10.1080/01621459.1988.10478560

402   Petrillo, G., & Lippiello, E. (2021). Testing of the foreshock hypothesis within an epidemic like
403   description of seismicity. *Geophysical Journal International*, *225*, 1236–1257.
404   https://doi.org/10.1093/gji/ggaa611

405   Ross, Z. E, Cochran, E. S., Trugman, D. T., & Smith, J. D. (2021). 3D fault architecture controls
406   the dynamism of earthquake swarms. *Science*, *368*(6497), 1357-1361.
407   https://doi.org/10.1126/science.abb0779

408   Seif, S., Zechar, J. D., Mignan, A., Nandan, S., & Wiemer, S. (2019). Foreshocks and Their
409   Potential Deviation from General Seismicity. *Bulletin of the Seismological Society of
410   America*, *109* (1), 1–18. https://doi.org/10.1785/0120170188

411   Taroni, M., Marzocchi, W., Schorlemmer, D., Werner, M. J., Wiemer, S., Zechar, J. D.,
412   Heiniger, L., & Euchner, F. (2018). Prospective CSEP Evaluation of 1-Day, 3-Month,
413   and 5-Yr Earthquake Forecasts for Italy. *Seismological Research Letters*, *89*, 1251-1261.
414   https://doi.org/10.1785/0220180031

415   Zaliapin, I., & Ben-Zion, I. (2013). Earthquake clusters in southern California I: Identification
416   and stability. *Journal of Geophysical Research: Solid Earth*, *118*, 2847-2864.
417   https://doi.org/10.1002/jgrb.50179

418   Zaliapin, I., & Ben-Zion, I. (2013). Earthquake clusters in southern California II: Classification
419   and relation to physical properties of the crust. *Journal of Geophysical Research: Solid
420   Earth*, *118*, 2865-2877. http://doi.org/10.1002/jgrb.50178

421   Zaliapin, I., Gabrielov, A., Keilis-Borok, V., & Wong, H. (2008). Clustering Analysis of
422   Seismicity and Aftershock Identification. *Physical Review Letters*, *101*, 018501.
423   https://doi.org/10.1103/PhysRevLett.101.018501

Geophysical Research Letters

Supporting Information for

Anomalous foreshock activity in southern California is associated with zones of high heat flow

Ester Manganiello[1], Marcus Herrmann[1], and Warner Marzocchi[1]

[1]University of Naples Federico II, Dept. of Earth, Environmental, and Resources Sciences, Italy

Contents of this file

Introduction

The supporting information contains additional information about the ETAS model used for the analyses and its verification.

It also reports the results using alternative methods to infer and select anomalous foreshock sequences (e.g., the spatiotemporal windows (STW) method to identify mainshocks and their foreshocks, using a significance level of 95%, using an alternative analysis of TEST1, and using an independent dataset).

Text S1. ETAS model

We used the stochastic ETAS aftershock simulator program developed by K. Felzer (see Felzer et al., 2002, Data Availability Statement, and Table S1) with parameters provided by Hardebeck et al., 2008, see Table S2). The program simulates background events, and triggered earthquakes in time and space. It makes use of Monte Carlo methods and empirical aftershock relationships following the ETAS model of Ogata (1988).

Text S2. Verifying the reliability of ETAS model

To verify the reliability of ETAS model, we adopt a Turing-style test (Page & van der Elst, 2018), comparing the number of earthquakes in the real catalog with the number of simulated events in the synthetic catalogs (Figure S1). We also apply the same kind of analysis to different

earthquake magnitude classes C_M = {3.0 ≤ M < 4.0, 4.0 ≤ M < 5.0, 5.0 ≤ M < 6.0, M ≥ 6.0} (Figure S2). In all cases, the real observation (solid vertical line) is within the 95% confidence interval (vertical dashed lines), indicating that the ETAS model is reliable and the synthetic catalogs consistent with the observation.

Text S3. Results for a significance level of 95%

Figures S6 shows the results of TEST1 using a significance level of 95%. Of a total of 152 foreshock sequences, we found 65 (43%) anomalous foreshock sequences using the NN method. Figure S7 shows the results for TEST2: we found 51 of 152 (36%) foreshock sequences to be anomalous using the NN method.

Table S1. Parameters used in K. Felzer's ETAS simulator.

Start date of simulation	1-1-1981
Start date of synthetic catalogs	1-1-1983
End date of synthetic catalogs	31-12-2019
Lower magnitude limit of active earthquakes, M_o	2.5
Lower magnitude limit in synthetic catalog	2.5
Lower magnitude limit for modelling planar sources	6.5
Upper magnitude limit	7.9
Minimum aftershock distance from parent event	0.001 (km)
Maximum aftershock distance from parent event	500 (km)

Table S2. Used ETAS parameters as given by Hardebeck et al., 2008 for M_o = 2.5. μ is the background rate; K, c, and p are parameters of Omori's law; n is the aftershock decay with distance (exponent in r^{-n}); α is the productivity law exponent (productivity scaling with magnitude); and β is the scaled b-value, $\beta = b * \ln(10)$, of the Gutenberg-Richter relation (describing the magnitude distribution).

μ	K	c	p	n	α, β
spatially variable	0.008	0.095	1.34	1.37	$\ln(10) \approx 2.30$

References

Felzer, K. R., Becker, T. W., Abercrombie, R. E., Ekstrom, G., & Rice, J.R. (2002). Triggering of the 1999 MW 7.1 Hector Mine earthquake by aftershocks of the 1992 MW 7.3 Landers earthquake, *Journal of Geophysical Research*: *Solid Earth*, *107*(B9), ESE 6-1–ESE 6-13. doi: 10.1029/2001JB000911.

Hardebeck, J. L., Felzer, K. R., and Michael, A. J. (2008), Improved tests reveal that the accelerating moment release hypothesis is statistically insignificant, *Journal of Geophysical Research*, *113*(B8). doi: 10.1029/2007JB005410.

Page, M. T., & van der Elst, N. J. (2018). Turing-Style Tests for UCERF3 Synthetic Catalogs, *Bulletin of the Seismological Society of America*, *108*(2), 729–741. doi: 10.1785/0120170223.
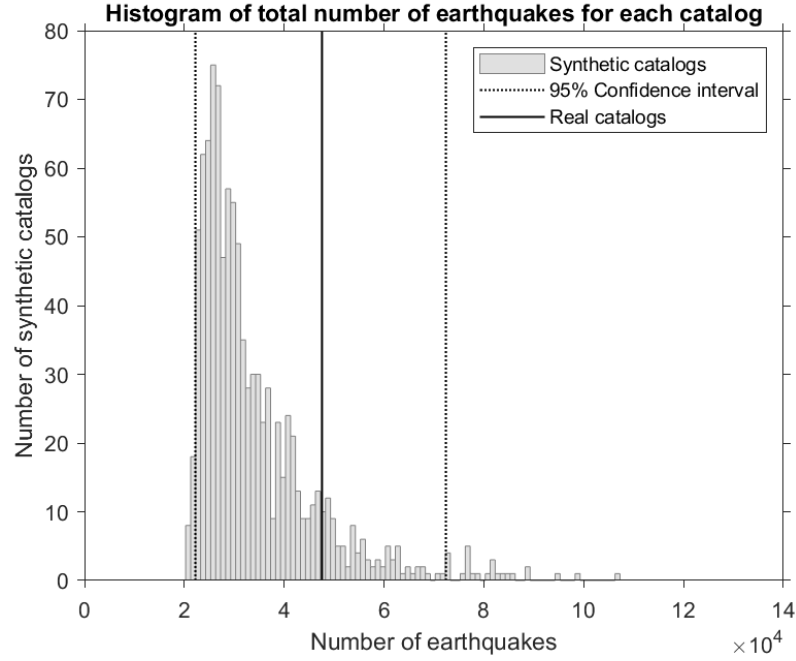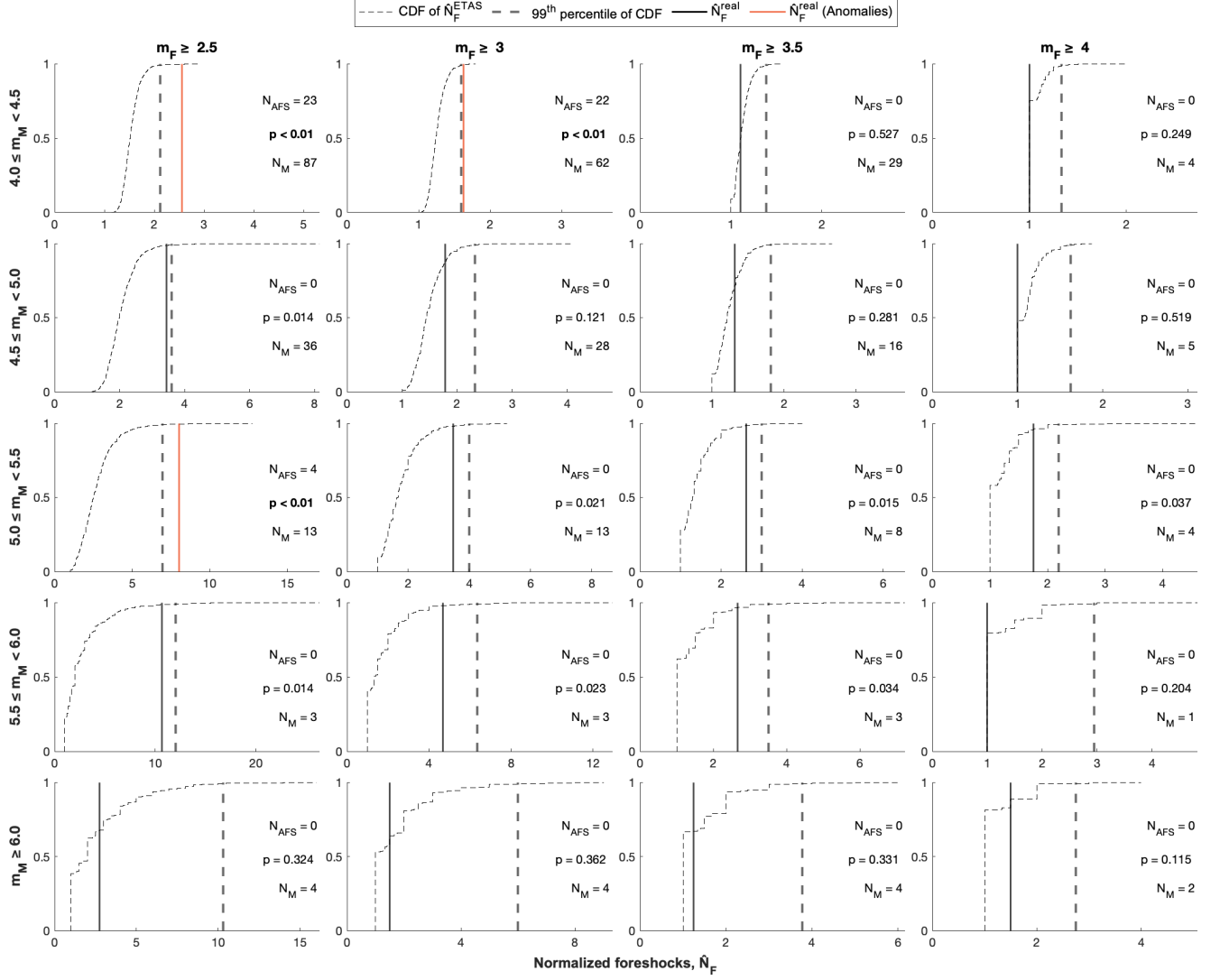
Figure S1. Total number of events in the synthetic catalogs (distribution) and the real catalog (solid vertical line). The dashed vertical lines refer to the 95% confidence interval (i.e., the 2.5^{th} – 97.5^{th} percentile range of the distribution). For more information, see Text S2.
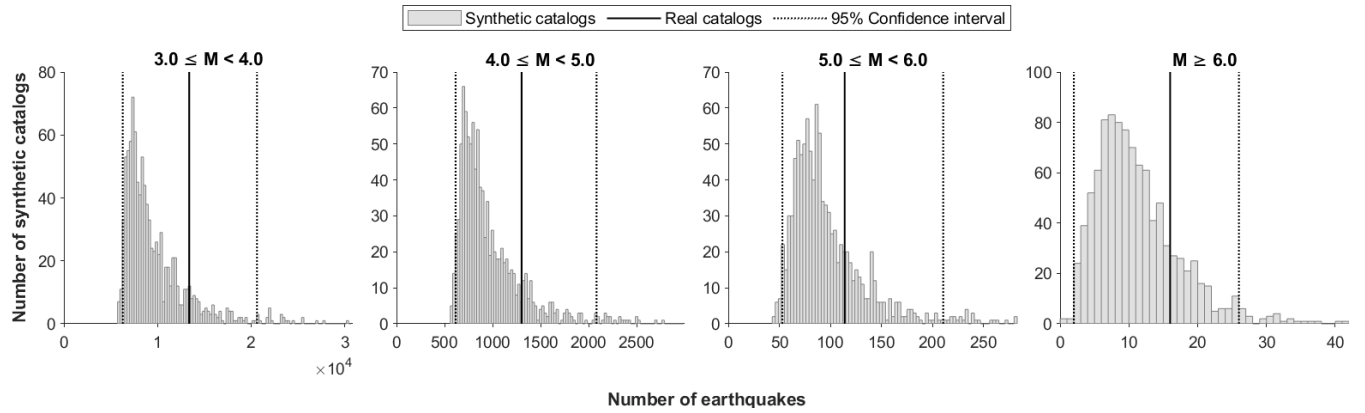
Figure S2. Like Figure S1 but for different magnitude classes.

Figure S3. Like Figure 1 in the main paper (TEST1) but using the STW method.
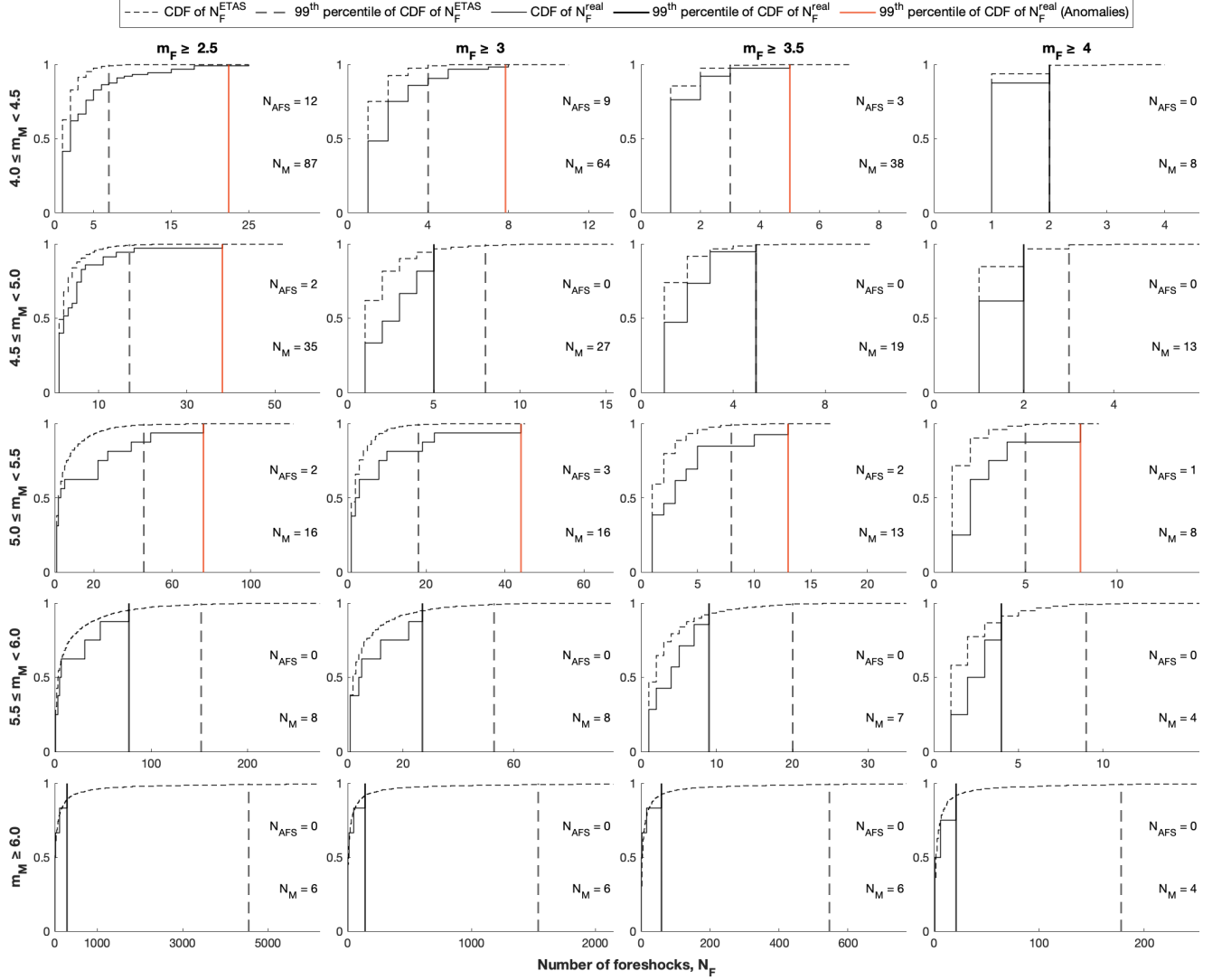
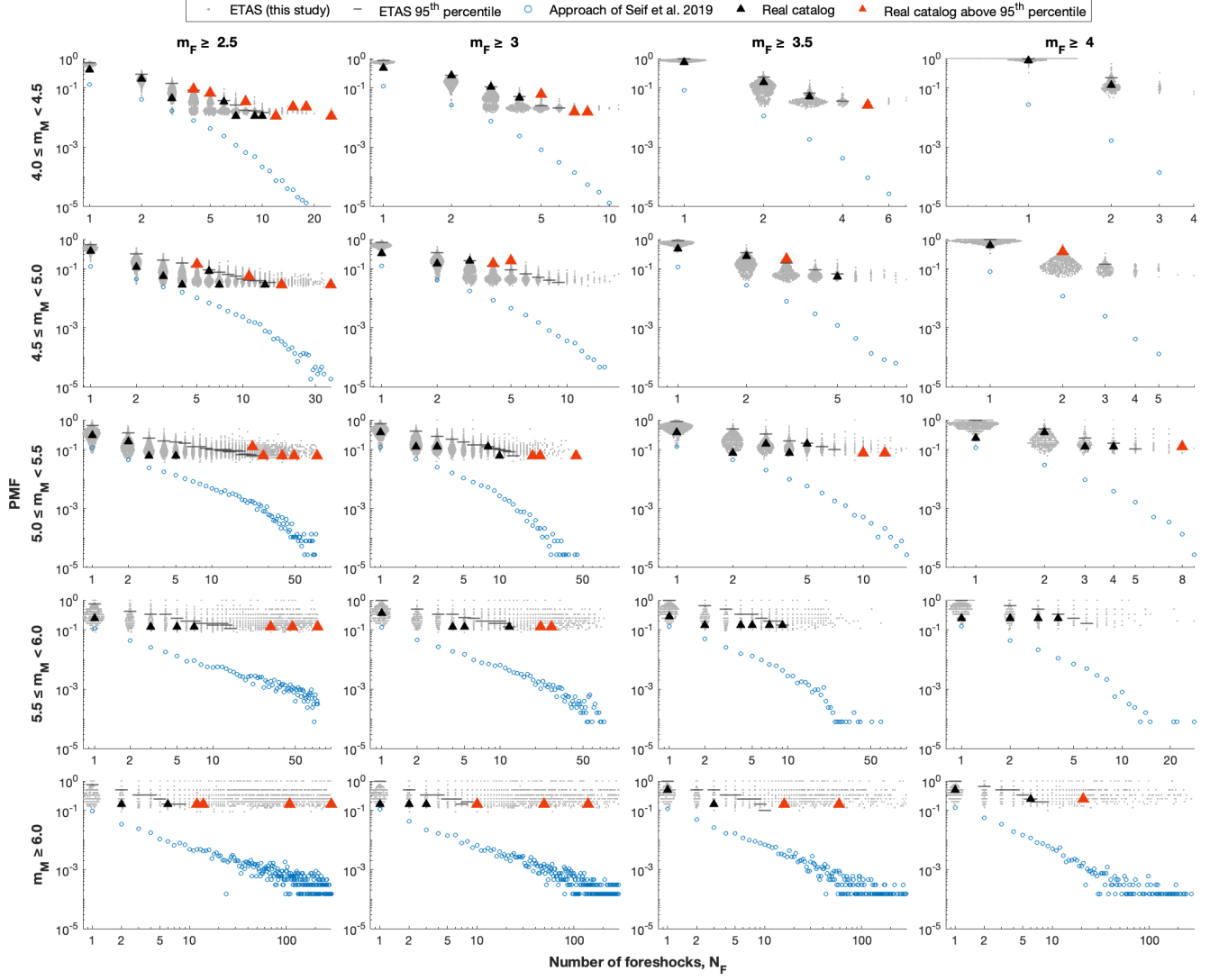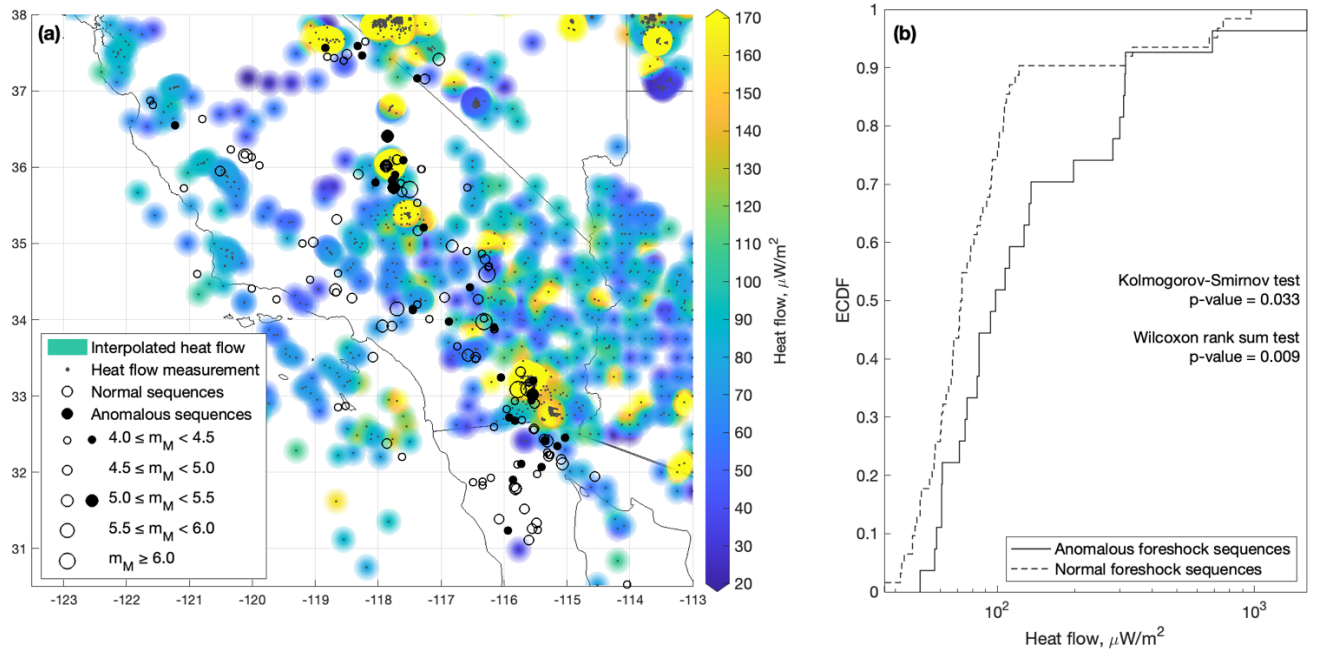**Figure S4** Like Figure 1 in the main paper (TEST1, NN method) but using the individual number of foreshocks, N_F. In this way, the empirical Cumulative Distribution Function (eCDF) of N_F can be constructed for both the real catalog (solid curve) and all 1000 synthetic catalogs combined (dashed curve); vertical lines show their corresponding 99th percentile (real catalog: solid; synthetic catalogs: dashed). If the former is above the latter, the solid vertical line becomes red, indicating more anomalous foreshock sequences than expected. Each subplot also reports the number of anomalous foreshock sequences, N_{AFS}, and the number of mainshocks, N_M.
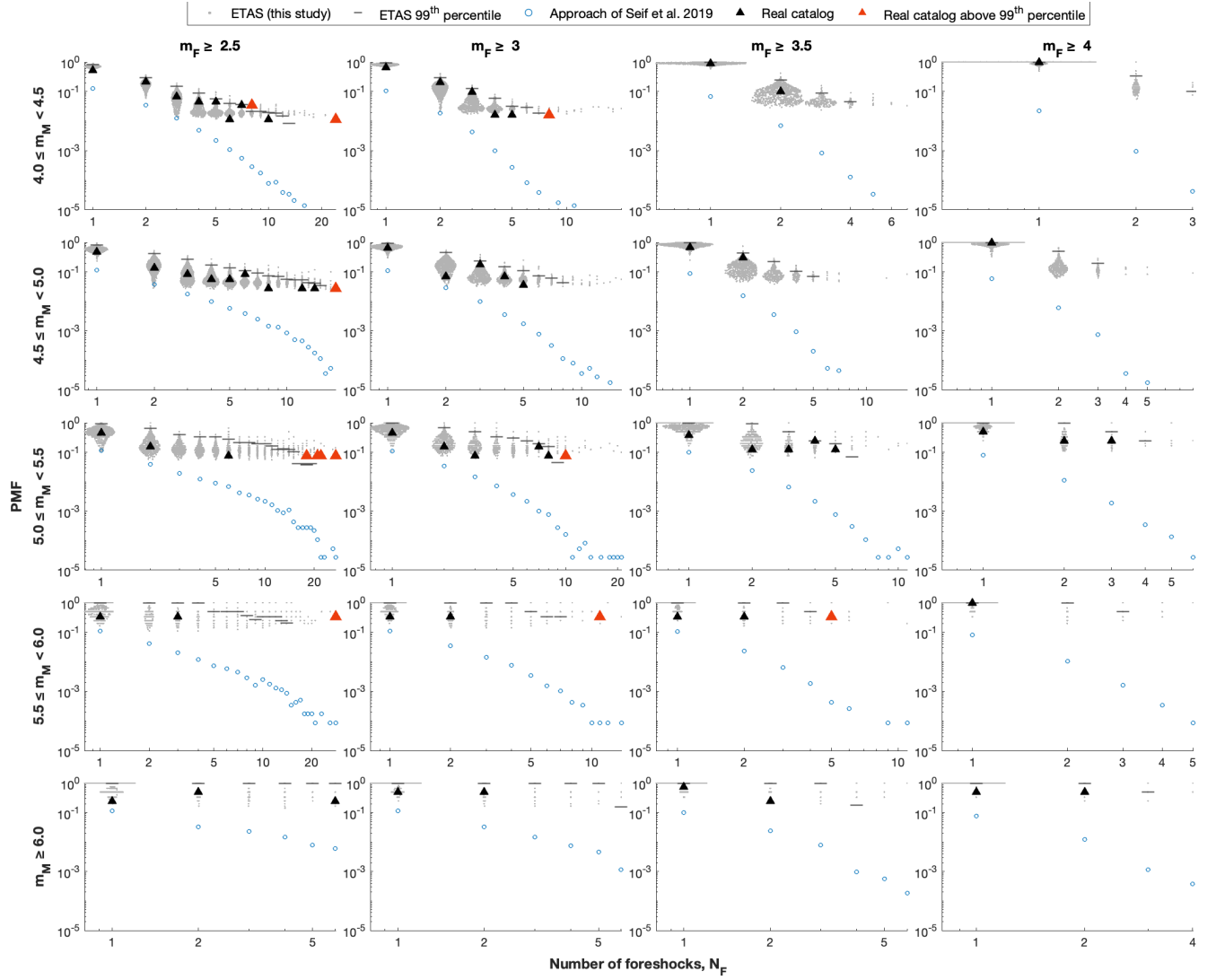
Figure S5. Like Figure 2 in the main paper (TEST2) but using the STW method.
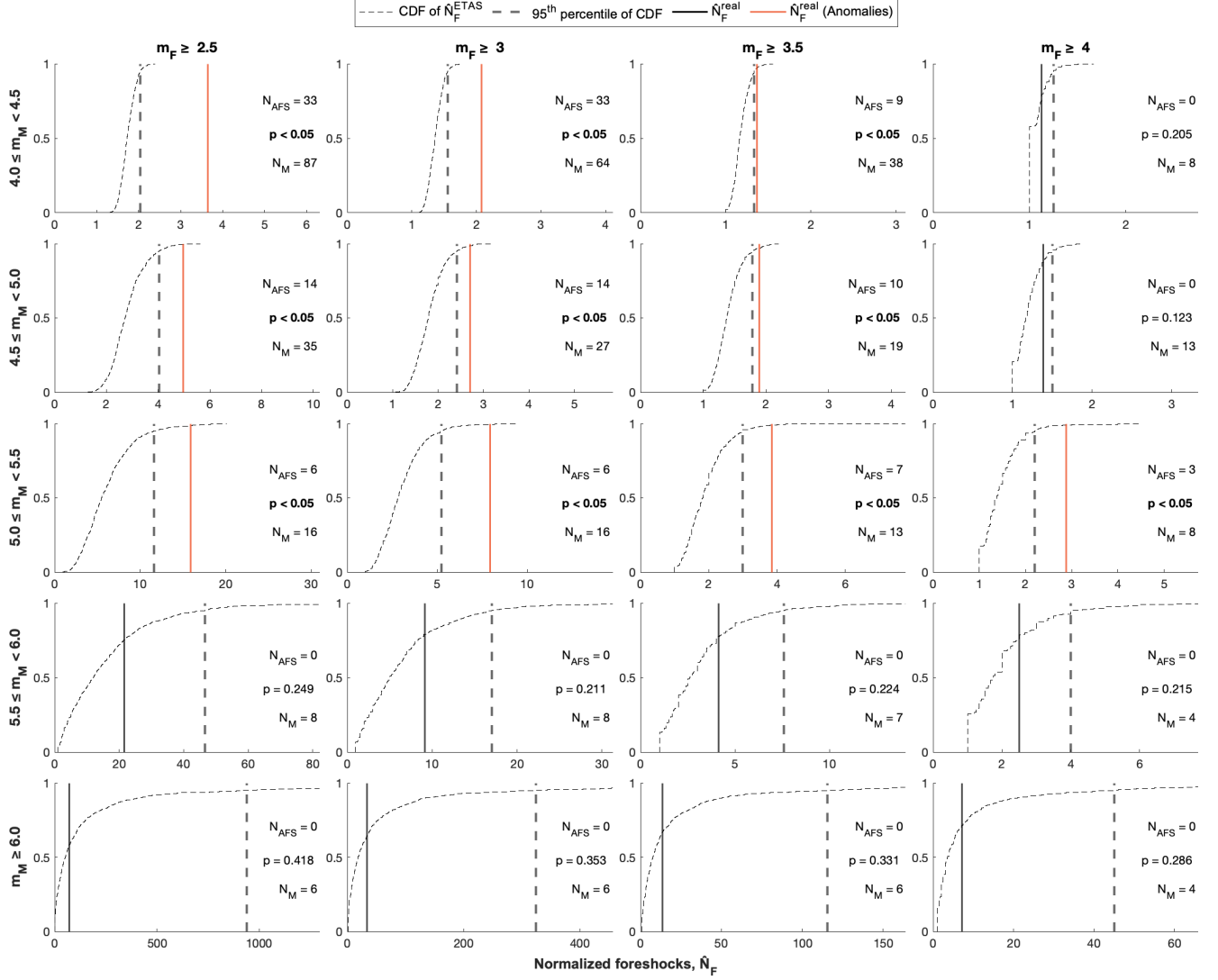
Figure S6. Like Figure 1 in the main paper (TEST1, NN method) but using a significance level of 95%.
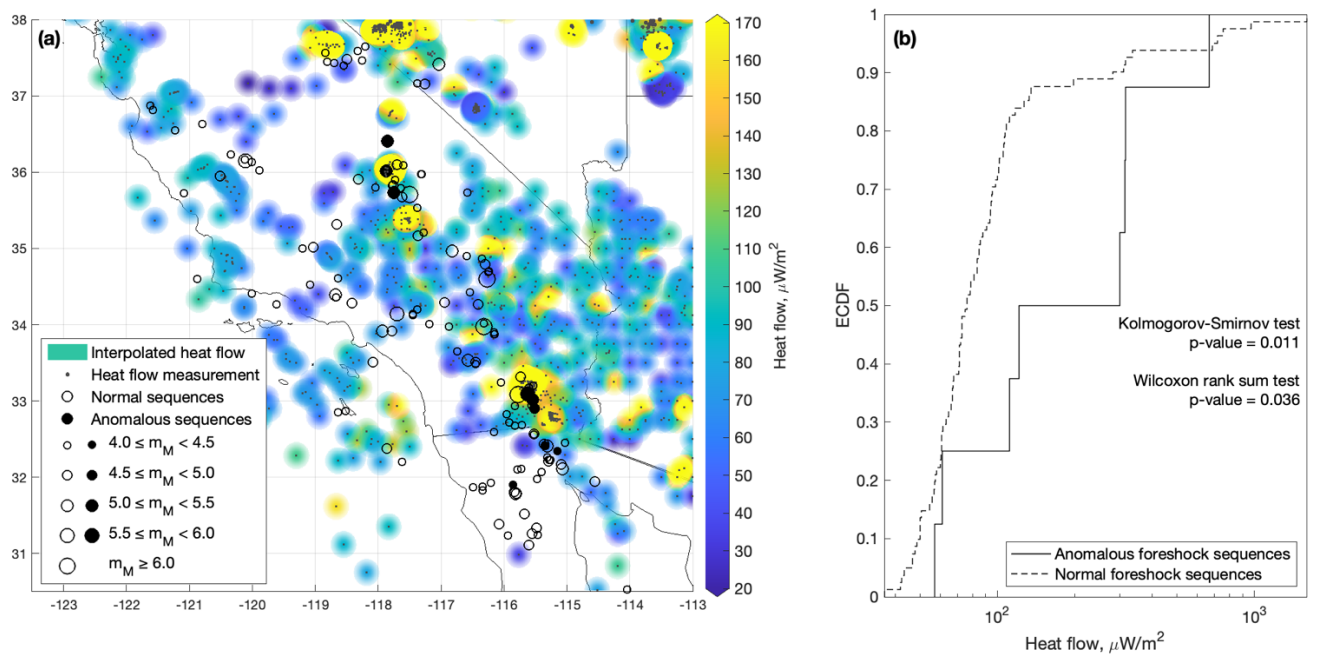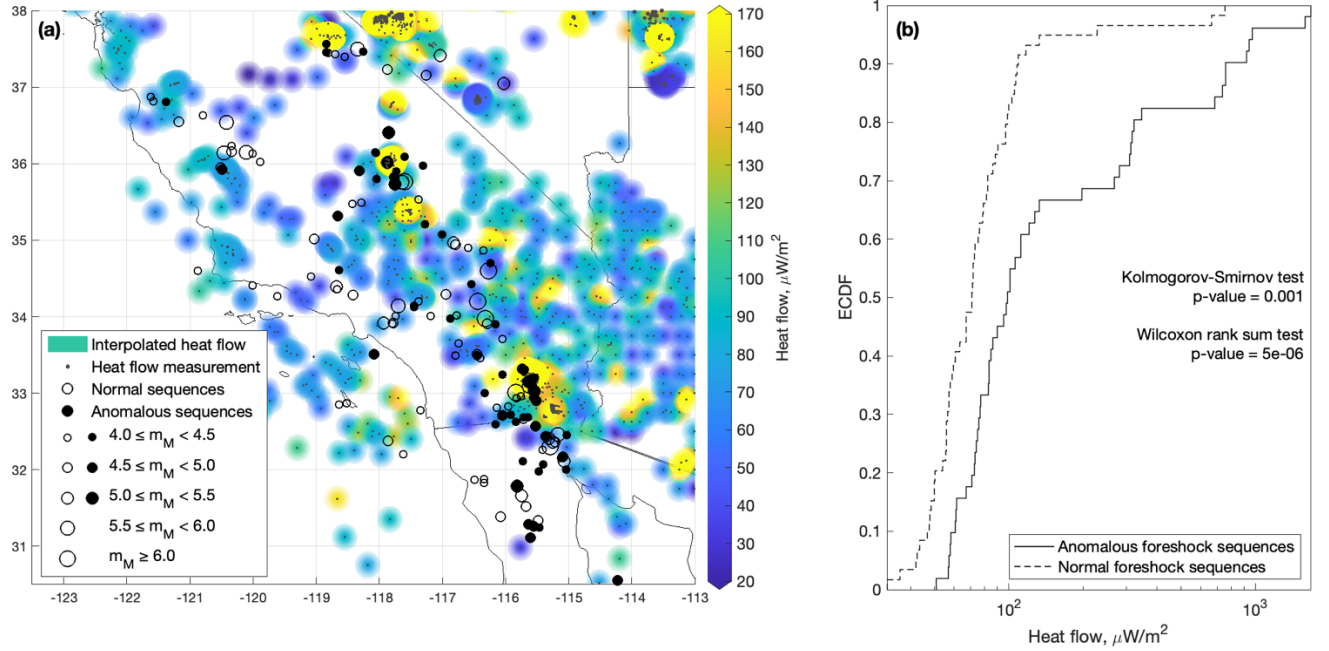
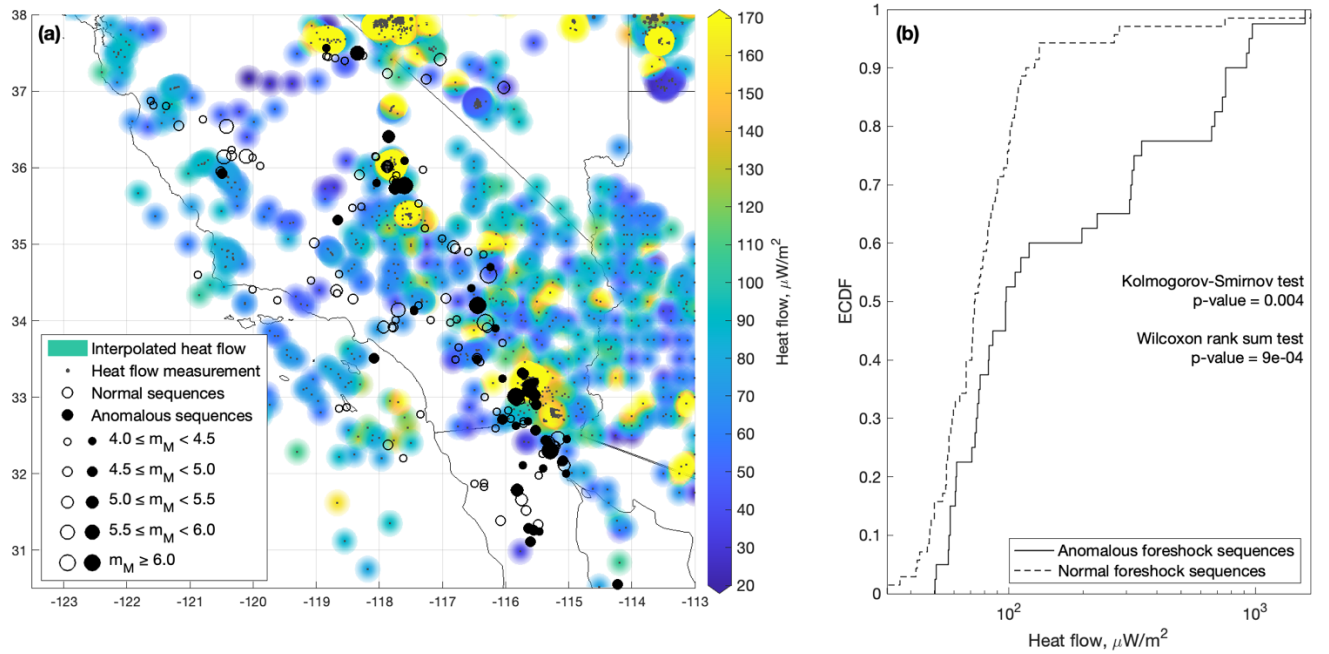**Figure S7.** Like Figure 2 in the main paper (TEST2, NN method) but using a significance level of 95%.

Figure S8. Like Figure 3 in the main paper (TEST1) but using the STW method.

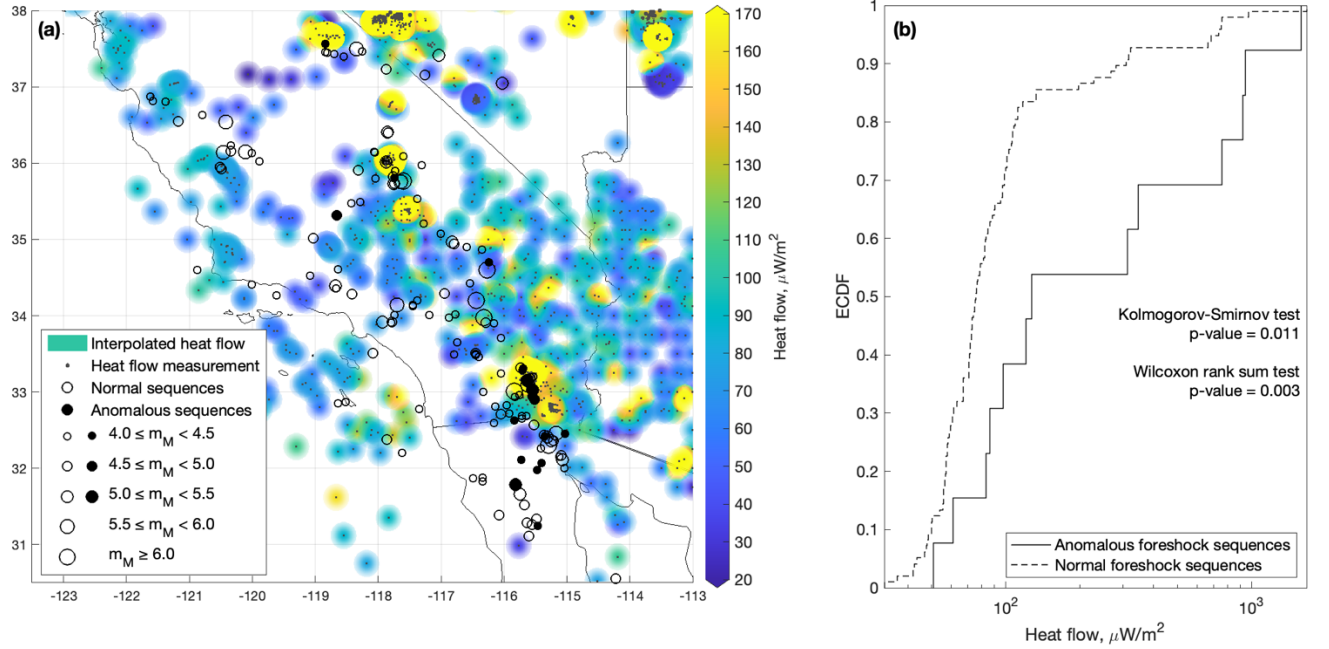**Figure S9.** Like Figure 4 in the main paper (TEST2) but using the STW method.

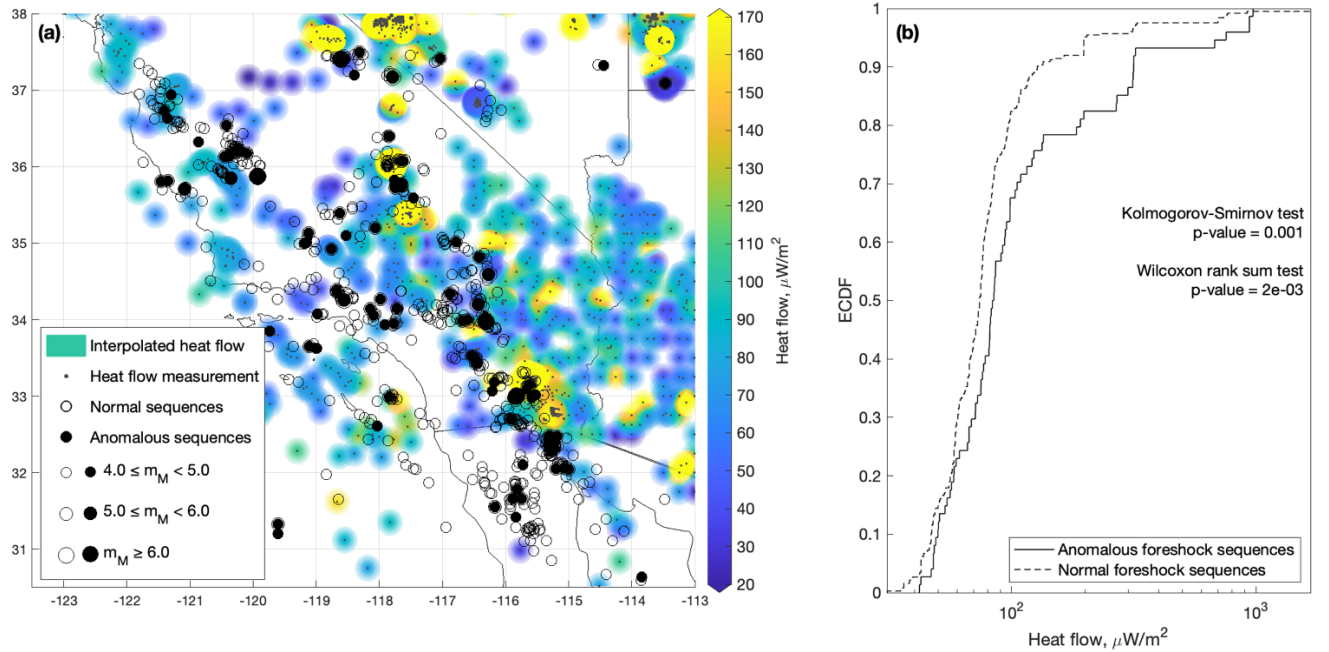**Figure S10.** Like Figure 3 in the main paper (TEST1, NN method) but using a significance level of 95%.

Figure S11. Like Figure 4 in the main paper (TEST2, NN method) but using a significance level of 95%.

Figure S12. Like Figure 3 in the main paper (TEST1, NN method, 99th percentile) but with anomalous sequences identified using an alternative analysis that uses the distributions of the individual number of foreshocks (not the average, see Figure S4).

Figure S13. Like Figure 3 in the main paper but with the locations of normal and anomalous foreshock sequences identified by Petrillo & Lippiello (2021).